Structures and Buildings
Volume 167 Issue SB3

Cyclic response of hollow and concrete-filled circular hollow section braces
Sheehan and Chan

ice | proceedings

Proceedings of the Institution of Civil Engineers
Structures and Buildings 167 March 2014 Issue SB3
Pages 140–152 http://dx.doi.org/10.1680/stbu.12.00033
Paper 1200033
Received 10/05/2012 Accepted 08/11/2012
Published online 01/02/2013
Keywords: buildings, structures & design/composite structures/seismic engineering

ice Institution of Civil Engineers publishing

Cyclic response of hollow and concrete-filled circular hollow section braces

1 **Therese Sheehan** MSc, DIC
PhD Candidate, School of Engineering, University of Warwick, Coventry, UK

2 **Tak-Ming Chan** MSc, DIC, PhD, CEng, MIStructE
Associate Professor, School of Engineering, University of Warwick, Coventry, UK

The behaviour of seismic-resistant buildings relies heavily upon the inclusion of energy dissipating devices. For concentrically-braced frames, this function is accomplished by diagonal bracing members whose performance depends upon both cross-sectional properties and global slenderness. Traditionally preferred rectangular hollow sections are susceptible to local buckling, particularly in cold-formed tubes, owing to the residual stresses from manufacture. This paper explores the response of hollow and concrete-filled circular tubes under cyclic axial loading. The uniformity of the circular cross-section provides superior structural efficiency over rectangular sections and can be further optimised by the inclusion of concrete infill. A series of experiments was conducted on filled and hollow specimens to assess the merit of the composite section. Comparisons were drawn between hot-finished and cold-formed sections to establish the influence of fabrication on member performance. Two specimen lengths were utilised to assess the influence of non-dimensional slenderness. Parameters such as ductility, energy dissipation, tensile strength and compressive resistance are presented and compared with design codes and empirically derived predictions.

Notation

A_a	steel cross-sectional area
A_c	concrete cross-sectional area
a, b, c	empirical constants (Tremblay, 2002)
C_u	maximum compressive resistance (CSA, 1994)
C'_u	post-buckling resistance
D	cross-section outer diameter
E	Young's modulus
F_y	steel yield strength (Equations 4–6)
f_{cd}	concrete design resistance (BSI, 2004a)
f_{yd}	steel design yield strength (BS EN 1993-1-1 (BSI, 2005), BS EN 1994-1-1 (BSI, 2004a))
L	specimen length
$N_{b,Rd}$	member buckling resistance
N_c	maximum brace compressive resistance per cycle (experiments)
$N_{c,max}$	maximum compressive resistance experiments
$N_{pl,Rd}$	cross-section compressive resistance
$N_{pl,test}$	maximum stub column load
N_t	maximum brace tensile resistance per cycle (experiments)
$N_{t,max}$	maximum tensile resistance (experiments)
$N_{t,y}$	predicted yield force from tensile tests
n	parameter for determining column compressive strength C_u
P_n	maximum compressive resistance (AISC, 2002)
r	steel strain-hardening parameter (Equation 6)
t	steel tube thickness
W_y	yield energy ($=f_{yd}A_a\delta_y$)
α, β	parameters for calculating post-buckling resistance (Nakashima *et al.*, 1992)
δ	axial displacement
δ_c	axial compressive displacement
δ_y	axial yield displacement
η_a	reduction parameter for steel resistance (BS EN 1994-1-1 (BSI, 2004a))
η_c	parameter to account for confinement effect in concrete (BS EN 1994-1-1 (BSI, 2004a))
$\bar{\lambda}$, λ	non-dimensional slenderness
μ_Δ	displacement ductility
σ_{ult}	ultimate stress (tensile coupons)
σ_y	steel yield stress (hot-finished)/0·2% proof stress (cold-formed)
Φ	confinement index (Cai, 1987)

1. Introduction

A variety of structural systems is used in seismic-resistant buildings to provide lateral stability and dissipate energy. Concentrically-braced frames (CBFs) are often selected as they are relatively simple to design in comparison with moment-resisting frames or eccentrically-braced frames (EBFs). The function of the diagonal braces in CBFs is to act as a structural 'fuse', dissipating the seismic energy through plastic deformation. Depending on the geometry of the frame, this may be achieved solely through tensile brace deformation (e.g. cross bracing) or through a combination of tensile and compressive brace deformation (e.g. chevron bracing). However, under repeated cycles of high axial displacement, the tensile and compressive resistances of braces decrease, particularly in the case of globally slender members, reducing the energy dissipation capability and potentially creating an unsymmetrical response in the framing system.

Rectangular hollow steel sections are usually selected as bracing members, and a significant amount of research has been carried out on these to date (e.g. Nip *et al.*, 2010), comparing the response of hot-rolled carbon steel, cold-formed carbon steel and stainless steel members. The cold-formed steel response was largely governed by the variation in residual stress between the corner and flat regions, and hot-rolled tubes displayed a superior performance overall. In addition to hollow sections, several researchers have explored the behaviour of concrete-filled rectangular tubes (e.g. Broderick *et al.*, 2005; Lee *et al.*, 2000; Liu and Goel, 1988). Concrete-filled tubular braces are becoming increasing popular as the contribution of concrete prevents inward deformation of the steel tube, enhancing the strength of these slender members.

In practice, other tubular section shapes are often overlooked. However, profiles such as circular hollow sections (CHSs) (Elchalakani *et al.*, 2003; Packer *et al.*, 2010) and, more recently, elliptical hollow sections (Chan *et al.*, 2010; Chan and Gardner, 2008, 2009) are attracting more attention owing to the aesthetics and potentially improved structural efficiency of these shapes. Elchalakani *et al.* (2003) and Packer *et al.* (2010) demonstrated that hollow circular steel members are highly suitable for use as bracing members and they are not as sensitive to local buckling as rectangular sections owing to their more uniform shape. The advantages of the circular section could be utilised further by using concrete infill, with the homogeneity of confining pressure on the concrete core providing the optimum cross-section.

This research thus compared the resistance of hollow and concrete-filled circular tubes of both hot-rolled and cold-formed steel. Compressive stub column tests were executed to examine the response of the composite cross-section. Subsequently, braces were subjected to cyclic axial loading in accordance with ECCS guidelines (ECCS, 1986). Two member lengths were compared

- intermediate-length braces with non-dimensional slenderness values in the region of 1·0 in accordance with BS EN 1993-1-1 (BSI, 2005) and BS EN 1994-1-1 (BSI, 2004a)
- longer members with non-dimensional slenderness values close to 2·0, which is the maximum limit imposed for braces in CBFs in BS EN 1998-1 (BSI, 2004b).

The main parameters considered were the ductility and energy dissipation potential of these sections in addition to the compressive and tensile resistance and deformed shape.

2. Material tests

2.1 Tensile coupons

Two types of circular hollow steel section were used – a hot-finished tube (Celsius 355) and a cold-formed section (Hybox 355). Nominal dimensions, yield stress and ultimate stress for these are summarised in Table 1. Stocky sections were selected to provide a high rotational capacity under repeated seismic actions. The D/t ratios for each cross-section give a cross-sectional classification of class 1 in accordance with BS EN 1993-1-1 (BSI, 2005).

Four longitudinal coupons were cut from each tube. One of these was located at the seam weld and the others were distributed at equal distances around the section circumference. Tensile coupon tests were carried out in accordance with BS EN ISO 6892-1 (BSI, 2009). The coupon ends were flattened prior to testing in order to fit inside the grips of the testing machine and hence they were dimensioned to mitigate the influence of work-hardening from this process on the central region. Resulting stress–strain relationships correlated closely to those expected, with the hot-rolled steel exhibiting linear behaviour up to yield, followed by a plateau before advancing to the strain-hardening region. In contrast, the cold-formed material was non-linear in the initial stages of the test and did not display a plateau during yield. The average yield stress (hot-rolled)/0·2% proof stress (cold-formed), ultimate stress, Young's modulus and percentage elongation after fracture are presented in Table 2, omitting the seam weld coupon results.

Steel	D: mm	t: mm	σ_y: N/mm^2	σ_{ult}: N/mm^2
Hot-finished	48·3	3·2	355	510
Cold-formed	48·3	3·0	355	470–630

Table 1. Nominal steel tube dimensions and material properties

Steel	σ_y: N/mm^2	σ_{ult}: N/mm^2	E: N/mm^2	Elongation after fracture: %
Hot-rolled	415	546	206000	37
Cold-formed	499	573	184000	30

Table 2. Results of tensile coupon tests

2.2 Concrete

The concrete mix was designed to meet two objectives. The first was a compressive strength of 20–25 MPa, to meet the minimum strength requirement of grade 20 for seismic applications as specified in BS EN 1998-1 (BSI, 2004b). Also, it has been found that concrete strengths greater than 28 MPa do not significantly enhance the behaviour (Liu and Goel, 1988). The second objective was to achieve satisfactory compaction for the long slender tubes without segregating the mix. A compaction procedure was developed by fixing the specimens vertically to a loosely bolted frame to which a beam vibrator was clamped. The tubes were filled in layers during continuous vibration of the frame and compaction was further aided by gently tapping the sides of the tube with a rubber mallet after each layer. The final concrete mix used a water/cement ratio of 0·72, a maximum aggregate size of 6·35 mm and had a high percentage of water and fine aggregate. The compressive strength on the test date was obtained in accordance with BS EN 12390-3 (BSI, 2002) in addition to the static elastic modulus. These values are given for each member type in Table 3.

3. Stub column tests

3.1 Test preparation

Compressive stub column tests were conducted to establish the degree of concrete confinement provided by each of the steel types and to characterise the cross-section that would later be utilised for the intermediate-length and long specimens. Eight stub columns were tested, all of which were 100 mm long.

Member	Compressive strength: N/mm^2	Static elastic modulus: N/mm^2
Stub column	25·5	19900
1500 mm brace	29·4	20100
3000 mm brace	30·7	23400

Table 3. Concrete properties at test date

Prior to testing, local imperfections were measured at 10 mm intervals along each of the four sides of the tube, along with the thickness and diameter. The specimen details and measured geometry are presented in Table 4. The nomenclature adopted for naming the specimens consists of three parts. The first part of the specimen ID refers to the steel-type – HF denotes hot-finished steel and CF refers to cold-formed steel. The second part distinguishes between hollow (H) and filled (F) specimens and the final part refers to the specimen type (SC = stub column in this case). Four longitudinal, post-yield strain gauges were used at the mid-height, allowing measurement of strains up to 15–20% elongation. Specimens were loaded initially under load control at a rate of 0·1 kN/s, switching to displacement control at yield.

3.2 Results

Most stub columns failed in a similar manner, with local buckling of the steel occurring at either the top or bottom of the specimen. Load–displacement relationships were derived for each of the test specimens, and examples of these are presented in Figure 1.

The hot-finished tubes exhibited a distinct yield plateau that was not observed for the cold-formed tubes. For the hollow stubs, the load decreased rapidly after reaching the ultimate value. However, the cold-formed filled specimen sustained a high load well beyond the failure of its hollow counterpart. Furthermore, the load–displacement curve for the hot-finished filled specimen continued to increase after specimen failure. This can be explained by the significant changes that propagated in the stub column geometry as the test progressed. As the axial displacement increased, the stub column buckled in a ring-shaped mode at two or more locations along the length, and these rings were eventually compressed together, becoming very stiff. The load–displacement relationship for the hot-finished concrete-filled tubes is consistent with the observations of Cai (1987) for thicker-walled steel tubes, after testing 57 concrete-filled circular stub columns. Following the approach of Cai (1987), the ultimate load in the case of the filled hot-finished stubs was defined as the load at the point of contra-flexure in the curve, as illustrated for specimen HF-F2-SC in Figure 1. This point signifies the transition

Specimen ID	Steel	Infill	Measured thickness: mm	Measured diameter: mm	Maximum imperfection: μm
HF-H1-SC	Hot-finished	—	3·17	48·64	45·02
HF-H2-SC	Hot-finished	—	3·19	48·58	57·77
CF-H1-SC	Cold-finished	—	2·82	48·66	27·82
CF-H2-SC	Cold-finished	—	2·85	48·65	35·50
HF-F1-SC	Hot-finished	Concrete	3·24	48·61	37·29
HF-F2-SC	Hot-finished	Concrete	3·23	48·60	27·65
CF-F1-SC	Cold-finished	Concrete	2·83	48·56	16·60
CF-F2-SC	Cold-finished	Concrete	2·85	48·61	22·22

Table 4. Stub column details

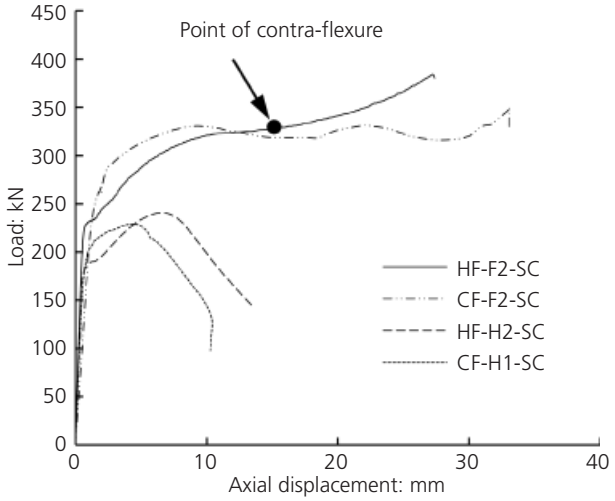

Figure 1. Load–displacement relationship for hot-finished and cold-formed stub columns

in the specimen response resulting from the altered geometry. BS EN 1994-1-1 (BSI, 2004a) predicts the ultimate compressive resistance of short concrete-filled circular tube-columns using

$$N_{\mathrm{pl,Rd}} = \eta_{\mathrm{a}} A_{\mathrm{a}} f_{\mathrm{yd}} + A_{\mathrm{c}} f_{\mathrm{cd}} \left(1 + \eta_{\mathrm{c}} \frac{t}{D} \frac{f_{\mathrm{yd}}}{f_{\mathrm{cd}}}\right) \quad 1.$$

For a loading eccentricity of zero

$$\eta_{\mathrm{a}} = 0{\cdot}25(3 + 2\bar{\lambda})$$

$$\eta_{\mathrm{c}} = 4{\cdot}9 - 18{\cdot}5\bar{\lambda} + 17\bar{\lambda}^2$$

Several other relationships have been proposed by researchers for the ultimate squash load of concrete-filled tubes. Following experiments involving specimens with a range of D/t ratios, Cai (1987) proposed the relationship

$$N_{\mathrm{pl,Rd}} = A_{\mathrm{c}} f_{\mathrm{cd}} (1 + \Phi^{1/2} + 1{\cdot}1\Phi) \quad 2.$$

where

$$\Phi = \frac{A_{\mathrm{a}} f_{\mathrm{yd}}}{A_{\mathrm{c}} f_{\mathrm{cd}}}$$

The maximum compressive loads are summarised in Table 5, in addition to the ratio of $N_{\mathrm{pl,test}}$ for each concrete-filled specimen to $N_{\mathrm{pl,test}}$ for the equivalent hollow section. The hot-finished hollow tubes significantly exceeded the predicted ultimate load in BS EN 1993-1-1 (BSI, 2005). The concrete infill enhanced the strength in all cases, with a greater increase in cold-formed than hot-finished, and this is also apparent in Figure 1. This is to be expected, since the cold-formed tube has a higher D/t ratio than the hot-finished and, hence, the concrete occupies a greater percentage of the cross-section. The maximum compressive strength shows very good agreement with predictions from BS EN 1994-1-1 (BSI, 2004a) and the work of Cai (1987).

4. Bracing tests

Following the stub column tests, cyclic axial tests were performed on 12 tubular braces.

4.1 Specimen preparation

Two specimen lengths were manufactured – an 'intermediate' specimen of 1500 mm length ($\bar{\lambda} = 0{\cdot}78$–$0{\cdot}92$) and a 'long' specimen of 3000 mm length ($\bar{\lambda} = 1{\cdot}72$–$2{\cdot}02$). Both hollow and filled braces were tested and a summary of these is provided in Table 6 along with non-dimensional slenderness values calculated in accordance with BS EN 1993-1-1 (BSI, 2005) and BS EN 1994-1-1 (BSI, 2004a). All members had fixed-end conditions and, hence, an effective length of $0{\cdot}7L$ was adopted (L being the original member length). This value was used to allow for imperfections in the boundary conditions of the test set-up. The identification convention is similar to that shown in Table 4, with the final part of the specimen ID referring to the bracing length. Guidance regarding brace slenderness in CBFs is provided by BS EN 1998-1 (BSI, 2004b) as

Specimen ID	$N_{\mathrm{pl,test}}$: kN	$N_{\mathrm{pl,test}}$ (filled)/$N_{\mathrm{pl,test}}$ (hollow)	$N_{\mathrm{pl,test}}/N_{\mathrm{pl,Rd}}$ (BSI, 2005/BSI, 2004a)	$N_{\mathrm{pl,test}}/N_{\mathrm{pl,Rd}}$ (Cai, 1987)
HF-H1-SC	234	—	1·24	—
HF-H2-SC	241	—	1·28	—
CF-H1-SC	237	—	1·11	—
CF-H2-SC	229	—	1·07	—
HF-F1-SC	325	1·37	1·05	1·01
HF-F2-SC	324	1·36	1·04	1·01
CF-F1-SC	331	1·42	0·96	0·93
CF-F2-SC	360	1·55	1·05	1·01

Table 5. Maximum loads from stub column tests

Specimen ID	Steel	Core	$\bar{\lambda}$	t: mm	Maximum global imperfection: mm	
					Unstiffened direction	Stiffened direction
HF-H-1500	Hot-finished	Hollow	0·78	3·18	0·58	0·49
CF-H-1500	Cold-formed	Hollow	0·90	2·83	0·62	0·73
HF-F1-1500	Hot-finished	Concrete-filled	0·81	3·21	0·26	0·37
HF-F2-1500	Hot-finished	Concrete-filled	0·81	3·20	0·22	0·38
CF-F1-1500	Cold-formed	Concrete-filled	0·92	2·85	0·67	0·73
CF-F2-1500	Cold-formed	Concrete-filled	0·92	2·82	0·67	0·61
HF-H-3000	Hot-finished	Hollow	1·72	3·19	1·88	1·84
CF-H-3000	Cold-formed	Hollow	1·98	2·81	2·95	3·86
HF-F1-3000	Hot-finished	Concrete-filled	1·78	3·19	1·50	1·52
HF-F2-3000	Hot-finished	Concrete-filled	1·78	3·22	1·30	1·34
CF-F1-3000	Cold-formed	Concrete-filled	2·02	2·82	3·27	2·27
CF-F2-3000	Cold-formed	Concrete-filled	2·02	2·84	3·46	2·76

Table 6. Summary of bracing specimens

$$1{\cdot}3 < \bar{\lambda} \leqslant 2{\cdot}0$$

for cross bracing and

$$\bar{\lambda} \leqslant 2{\cdot}0$$

for other configurations

All concrete-filled specimens were cast with the same concrete mix and compacted as described in section 2.2. Both hollow and concrete-filled tubes were then welded onto 25 mm thick steel end plates. To ensure structural integrity of the welded end connections, two stiffening plates with dimensions of 125 mm × 50 mm × 8 mm were also welded onto the outside of each tube at these locations.

The surface profile was measured along each of four faces. The maximum global imperfections in directions parallel to and perpendicular to the plane of the end stiffeners are included in Table 6 along with the average measured tube wall thickness.

4.2 Test procedure

Specimens were subjected to the cyclic loading protocol outlined by ECCS (1986), facilitating a direct comparison with the results of Nip *et al.* (2010) and Broderick *et al.* (2005). This loading sequence does not represent a real earthquake but was developed as a standardised procedure to establish the response of individual elements, substructures or entire structures under cyclic loading, since the behaviour of steel can deviate from the idealised elasto-plastic response after repeated loading cycles. In this case, the test was executed on an individual brace and the loading was applied directly to the member in order to represent part of the seismic action that would be experienced by this component within a complete structure. The loading procedure was symmetric in compression and tension, consisting of one displacement cycle at amplitudes $0{\cdot}25\delta_y$, $0{\cdot}5\delta_y$, $0{\cdot}75\delta_y$ and $1{\cdot}0\delta_y$ followed by three displacement cycles at each of $2\delta_y$, $4\delta_y$, $6\delta_y$, $8\delta_y$, etc. up to failure, where δ_y is the yield displacement of the specimen. This parameter was determined by using the values of yield stress/0·2% proof stress and Young's modulus, which were obtained from the tensile coupon tests to establish a quantity of yield strain, which was then multiplied by the member length to convert to displacement. In each cycle, specimens were first loaded in compression and then in tension.

A vertical purpose-built test-rig was constructed for the tests (Figure 2). Specimens were connected to the test-rig using six grade 8·8 M16 bolts at each end and cyclic displacements were applied with a 50 t hydraulic actuator. Load was measured using an inbuilt load cell and axial displacement was monitored with a linear variable displacement transducer (LVDT). Lateral displacements at mid-height were measured using string potentiometers, in the plane of the frame and the orthogonal direction, corresponding to the stiffened and unstiffened axes of the specimen ends. Longitudinal, post-yield strain gauges were utilised at the anticipated locations of plastic hinges: at the mid-length and close to the end fixtures. Displacement of the top beam was also measured throughout the tests to account for the flexibility of the test-rig. Although fully restrained boundary conditions were assumed at the specimen ends, two inclinometers were employed to monitor any rotations – one in the plane of the frame and the other in the orthogonal direction.

4.3 Deformation and failure

Each of the test specimens buckled globally about the unstiffened axis. As the axial displacement increased, so did the mid-height lateral displacement in the compression half of each cycle, until

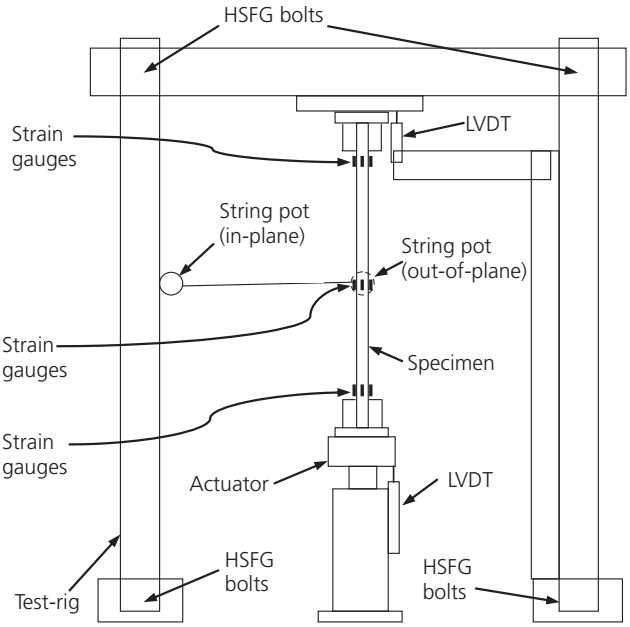

Figure 2. Test-rig and instrumentation

local buckling propagated in one or more of the anticipated plastic hinge regions. Specimens eventually failed by rupture of the steel tube at the location of local buckling in the tensile half of the cycle. Hot-finished and cold-formed hollow specimens underwent inward local buckling at the mid-height, as shown in Figure 3(a). Relatively little local deformation occurred in the hollow tubes other than at the mid-height.

The 1500 mm long concrete-filled specimens took on a more curved profile in comparison with the hollow specimens, which were effectively divided into two straight segments by the mid-height portion. This delayed the onset of local buckling for the concrete-filled specimens. In addition to that at mid-height, local buckling also occurred close to the ends of the concrete-filled specimens, but the buckling propagated outwards, increasing the section bending capacity. This, in addition to the improved distribution of plasticity along the length, enabled the concrete-filled specimens to endure a larger number of cycles than the hollow tubes.

Specimen HF-F1-1500 showed necking and outward local buckling at the base and mid-height, and eventually ruptured at these locations (Figure 3(b)). Specimens HF-F2-1500, CF-F1-1500 and CF-F2-1500 exhibited similar responses to HF-F1-1500. HF-F2-1500 eventually ruptured close to the top, and CF-F1-1500 and CF-F2-1500 failed adjacent to the base.

The 3000 mm long hollow specimens showed similar behaviour to the 1500 mm hollow specimens, but some differences were observed in the filled specimens. For the hot-finished filled tests, the maximum actuator stroke was reached before specimen

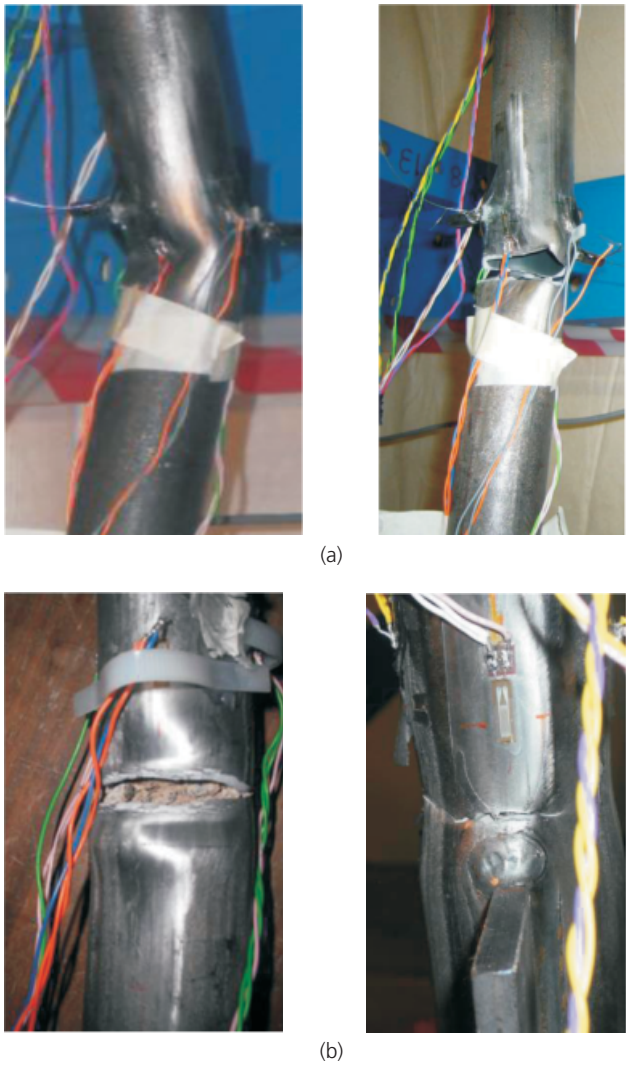

Figure 3. Deformation and failure: (a) mid-height of HF-H-1500; (b) mid-height and base of HF-F1-1500

failure had occurred. After three cycles at a displacement amplitude of $14\delta_y$, there were no obvious signs of local buckling and, hence, it is difficult to predict when failure would have occurred. For the cold-formed filled tests, some evidence of local buckling and necking was observed at the mid-height and close to the ends prior to fracture, but this was not as severe as in the case of the shorter tubes.

For the hot-finished sections, lateral deflection occurred predominantly about the unstiffened axis, but the cold-formed sections showed significant lateral displacements in both directions. Possible causes of this are the residual stresses in the cross-section from the cold-forming process or increased sensitivity to the global imperfection in the stiffened plane owing to the position of the seam weld. However, this cannot be confirmed without further experimental work.

4.4 Displacement ductility

Displacement ductility, μ_Δ is defined in this study as the ratio of maximum axial displacement to yield displacement, similar to the definition used by Nip *et al.* (2010). Table 7 summarises the total number of cycles to fracture and displacement ductility for each of the specimens. For both specimen lengths, the hot-finished tubes endured a greater number of cycles than the cold-formed specimens, and concrete-filled showed superior performance to the hollow specimens. In most cases, however, the filled specimens failed at the same displacement amplitude as the hollow specimens, but in a later cycle, and hence the benefits of concrete infill are not apparent in the values of μ_Δ. As discussed in section 4.3, it is expected that HF-F1-3000 and HF-F2-3000 would have surpassed the displacement ductility of their hollow counterpart. The concrete infill therefore appears to contribute more to μ_Δ for hot-finished than for cold-formed specimens.

4.5 First-cycle buckling loads

The first-cycle buckling loads are presented in Table 8 and Figure 4. Non-dimensional slenderness values ($\bar{\lambda}$) and buckling loads were calculated using buckling curve 'a' from BS EN 1993-1-1 (BSI, 2005) for hot-rolled and concrete-filled tubes and BS EN 1993-1-1 buckling curve 'c' for the hollow cold-formed tubes. In all cases, the values exceeded those predicted by BS EN 1993-1-1 or EN 1994-1-1, particularly for the longer members.

For all 1500 mm tubes, overall member buckling occurred in the fifth cycle, whereas for the 3000 mm tubes, this was in the third cycle, with the exception of HF-H-3000, which was in the fourth loading cycle. The overall trend shows some similarities to Nip *et al.* (2010), in which global buckling occurred between the third and fifth cycles, with specimens of higher $\bar{\lambda}$ generally buckling earlier. It is evident in Figure 4 that the first-cycle peak buckling load is enhanced by the presence of concrete infill for the 'intermediate-length' specimens.

Specimen ID	$\bar{\lambda}$	Number of cycles to fracture	μ_Δ
HF-H-1500	0·78	17	10
CF-H-1500	0·90	14	8
HF-F1-1500	0·81	28	16
HF-F2-1500	0·81	19	10
CF-F1-1500	0·92	15	8
CF-F2-1500	0·92	16	8
HF-H-3000	1·72	24	14
CF-H-3000	1·98	17	10
HF-F1-3000	1·78	25[a]	14
HF-F2-3000	1·78	25[a]	14
CF-F1-3000	2·02	17	10
CF-F2-3000	2·02	18	10

[a] Test terminated at actuator stroke limit.

Table 7. Maximum numbers of cycles and loads

Specimen ID	$\bar{\lambda}$	Cycle of global buckling	$N_{c,max}$: kN	$N_{c,max}/N_{b,Rd}$
HF-H-1500	0·78	5	155	1·17
CF-H-1500	0·90	5	151	1·43
HF-F1-1500	0·81	5	174	1·14
HF-F2-1500	0·81	5	175	1·15
CF-F1-1500	0·92	5	174	1·18
CF-F2-1500	0·92	5	164	1·11
HF-H-3000	1·72	4	81	1·47
CF-H-3000	1·98	3	71	1·66
HF-F1-3000	1·78	3	83	1·36
HF-F2-3000	1·78	3	88	1·44
CF-F1-3000	2·02	3	72	1·33
CF-F2-3000	2·02	3	71	1·32

Table 8. First-cycle buckling loads

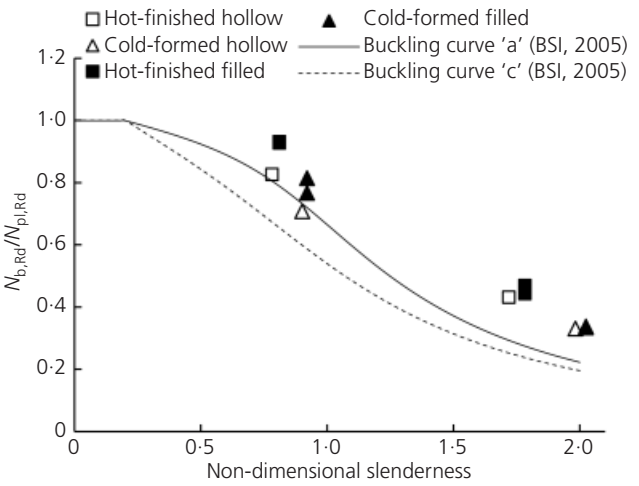

Figure 4. First-cycle buckling loads

4.6 Post-buckling compressive strength

Following on from the initial buckling behaviour, the next parameter to consider is reduction in compressive resistance up to the maximum compression displacement. This becomes significant in chevron-braced frames because the degradation of compressive strength may occur prior to yielding in the tensile brace, inducing a net vertical force on the connecting beam. Degradations of compressive resistance are presented in Figures 5(a) and (b) in relation to axial displacement for both 1500 mm and 3000 mm specimens in their first cycle at each amplitude. For the 1500 mm specimens, the presence of concrete infill increases the initial compressive strength. The compressive strength degradation at low displacement amplitudes ($\delta/\delta_y < 5$) is greater for the

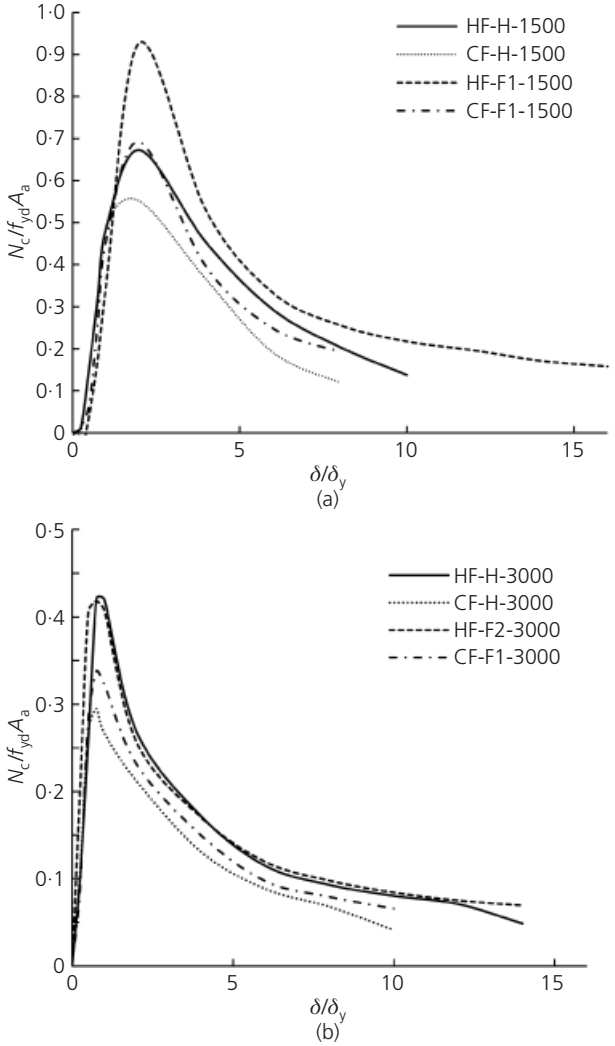

Figure 5. Post-buckling resistance in first cycle at each displacement amplitude: (a) 1500 mm specimens; (b) 3000 mm specimens

concrete-filled specimens than the hollow specimens, but this trend is reversed at higher displacement amplitudes ($\delta/\delta_y \geq 5$) for both hot-finished and cold-formed tubes. The concrete core has less impact on this parameter for the 3000 mm specimens, as illustrated in Figure 5(b). Similar behaviour was observed for the second and third cycles at each displacement amplitude.

A number of predictions have been made regarding the post-buckling compressive strength of seismic steel braces. AISC (2002) guidelines assume a value of $0{\cdot}26P_n$, where P_n is the estimated maximum axial compressive strength. CSA (1994) guidelines provide a prediction of buckling resistance in terms of the global slenderness

$$C'_u = \frac{C_u}{1 + 0{\cdot}35\bar{\lambda}} \quad (3)$$

where C_u is the maximum compressive resistance given by

$$C'_u = A_a F_y \left(\frac{1-\alpha\beta}{1-\beta}\right)^{4/3} \leq C_u \quad (4)$$

where $n = 1{\cdot}34$.

Tremblay (2002) developed an expression for post-buckling resistance based on results from 76 specimens, including a variety of cross-section shapes. The sections used were class 1 as these are most suitable for providing the required ductility under seismic loading. Tremblay's expression for post-buckling resistance is

$$C'_u = A_a F_y (a + b\bar{\lambda}^{-c}) \leq C_u \quad (5)$$

where values for a, b, and c were obtained from test data.

Nakashima *et al.* (1992) proposed

$$C'_u = A_a F_y \left(\frac{1-\alpha\beta}{1-\beta}\right)^{4/3} \leq C_u \quad (6)$$

where

$$\alpha = \frac{8r^{3/4}}{5\bar{\lambda}^{3/2}}$$

$$\beta = \alpha^{1/3} - \left(\alpha^{2/3} + \frac{5}{3}\bar{\lambda}^2 \frac{\delta_c}{\delta_y}\right)^{1/2}$$

Figures 6, 7 and 8 compare the experimental results with these predictions for displacement ductilities (μ_Δ) of 2, 3 and 5 respectively. These values of μ_Δ were selected following Tremblay (2002) in order to cover the range of expected axial deformations for braces in symmetrical tension–compression configurations. The data show satisfactory agreement with the CSA (1994) predictions under low displacement ductilities, but deviate towards the predictions of Tremblay (2002) and Nakashima *et al.* (1992) as μ_Δ increases. The AISC (2002) prediction is over-conservative in all cases. The concrete-filled tubes have significantly better post-buckling resistance for low values of $\bar{\lambda}$, but this difference becomes negligible as $\bar{\lambda}$ increases. Shorter members undergo more severe post-buckling resistance degradation than the longer braces as axial displacement increases, and this is evident in Figures 6 to 8.

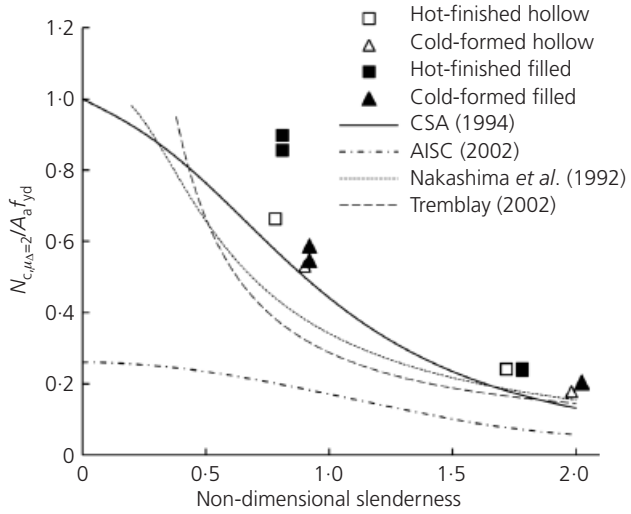

Figure 6. Relationship between post-buckling resistance and non-dimensional slenderness at $\mu_\Delta = 2$

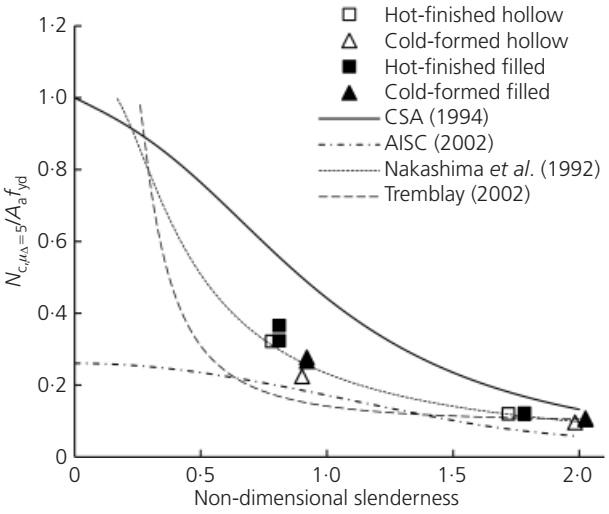

Figure 8. Relationship between post-buckling resistance and non-dimensional slenderness at $\mu_\Delta = 5$

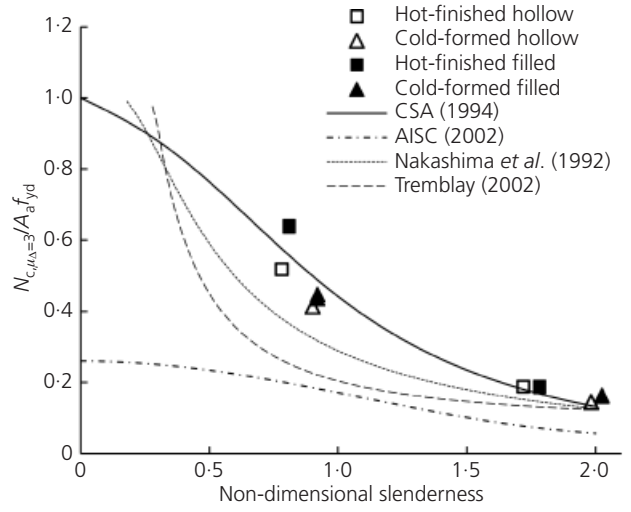

Figure 7. Relationship between post-buckling resistance and non-dimensional slenderness at $\mu_\Delta = 3$

Specimen ID	$N_{t,max}$: kN	$N_{t,max}/N_{t,y}$	Enhancement in $N_{t,max}$ from concrete: %
HF-H-1500	180	0·96	—
CF-H-1500	209	0·98	—
HF-F1-1500	198	1·05	10·0
HF-F2-1500	198	1·05	10·0
CF-F1-1500	220	1·03	5·3
CF-F2-1500	216	1·01	3·3
HF-H-3000	187	1·00	—
CF-H-3000	209	0·98	—
HF-F1-3000	203	1·08	8·6
HF-F2-3000	198	1·05	5·9
CF-F1-3000	223	1·05	6·7
CF-F2-3000	227	1·05	8·6

Table 9. Maximum tensile forces

4.7 Tensile load degradation

The maximum tensile resistances for each specimen are presented in Table 9 and compared with the yield strength of the steel cross-section. The concrete-filled specimens have better tensile resistance than the hollow members for both steel types. The concrete core provides some degree of tensile strength prior to cracking, but this observation can also be attributed to the prevention of inward deformation of the steel tube. Filled and hollow specimen results are compared in order to evaluate the contribution of concrete. Intermediate-length hot-finished tubes exhibit the greatest improvement, showing a 10% difference between filled and hollow resistances, whereas intermediate cold-formed specimens exhibit the least enhancement, with an average of 4·3%.

Tensile load degradations are presented for the 3000 mm test specimens in the first displacement cycle at each amplitude in Figure 9. Not only does the concrete increase the maximum tensile strength in the early stages of the test, but it maintains this enhancement as the protocol progresses. Similar trends were seen for the second and third cycles at each amplitude and for the shorter test specimens. Given the likelihood of concrete cracking early in the loading procedure, this result supports the suggestion that prevention of inward tubular deformation enhances the response in tension as well as in compression.

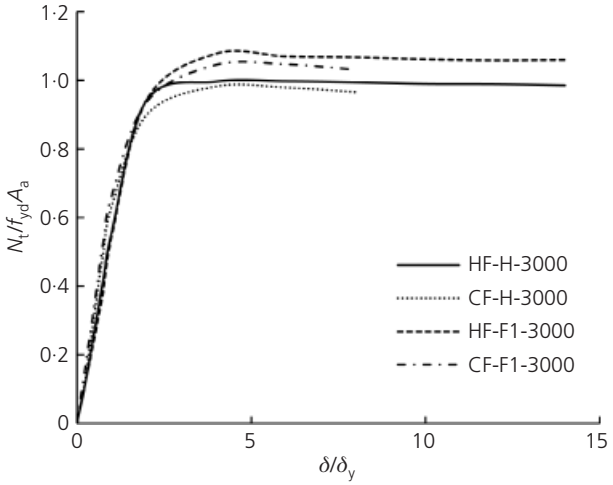

Figure 9. Maximum tensile force for first cycle at each displacement amplitude

4.8 Energy dissipation

Energy dissipation is defined in this paper as external work and is equal to the area enclosed by the load–displacement hysteresis loops. Curves for four of the test specimens are presented in Figures 10 and 11.

Similar hysteresis behaviour was seen for each test specimen. The specimens exhibited high stiffness under compressive loading, followed by gradual degradation after buckling. As loading is reversed into tension, specimens initially showed low stiffness owing to straightening of the member, which elongated in previous cycles. The increase in length and residual out-of-straightness account for the apparent tensile resistance reduction in the second and third cycles at each amplitude. The lengthening of the member in the first cycle of a particular displacement amplitude also reduces the buckling resistance in the compressive half of the second and third cycles.

The shorter test specimens (Figures 10(a) and (b)) enclose a larger area per hysteresis loop relative to δ_y than the more slender braces. Figure 12 presents the load–displacement relationship during the thirteenth cycle for both hollow and filled cold-formed tubes of each length. Some differences were apparent between the concrete-filled and hollow 1500 mm specimens, with the filled specimen hysteresis loop enclosing a greater area than the hollow, indicating more energy dissipated per cycle. However, this was not as noticeable for the 3000 mm specimens shown in the same figure. Furthermore, the concrete had less influence on the hysteresis shape for hot-finished tubes of either length. Overall, the results indicate that concrete infill does not greatly enhance the energy per cycle but does increase the total energy dissipation, owing to the number of cycles endured. Although the specimen life was generally only prolonged by one or two cycles, the maximum energy dissipation occurred within the later cycles

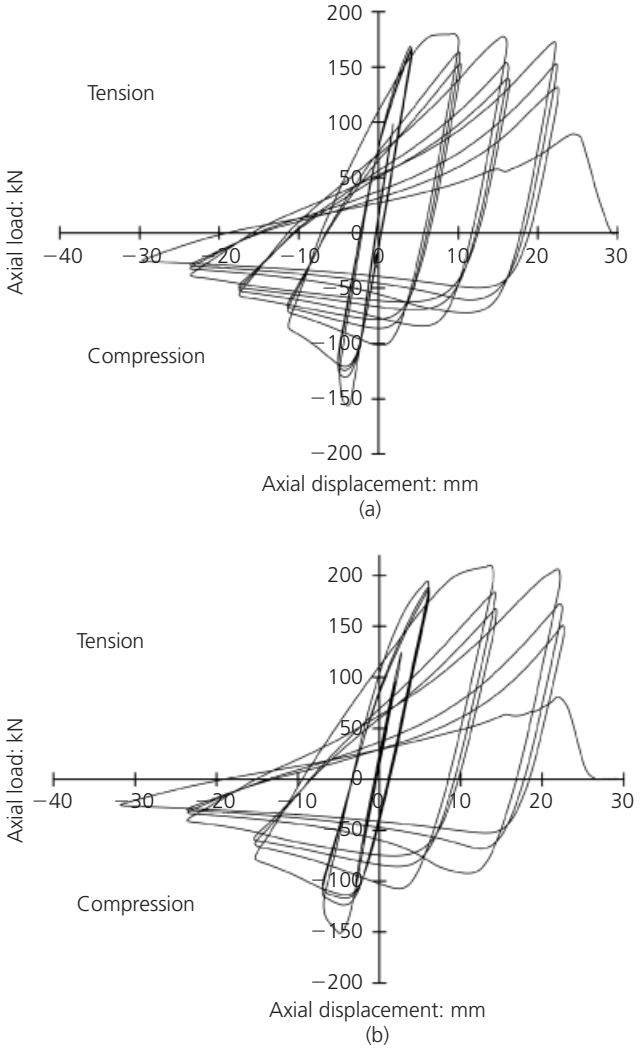

Figure 10. Load–displacement response for 1500 mm hollow specimens: (a) HF-H-1500; (b) CF-H-1500

of each test and, hence, the concrete contribution noticeably enhanced the total accumulated energy dissipation.

Table 10 lists the normalised energy dissipation in a number of individual test cycles and the total accumulated energy dissipation. The values in the table are normalised with respect to $W_y = f_{yd}A_a\delta_y$, the product of the steel yield stress, cross-sectional area and yield displacement of the member. The energy dissipated in the eighth loading cycle was examined by Nip *et al.* (2010) and Goggins *et al.* (2005) (this was the cycle with the greatest degree of energy dissipation for the majority of specimens). Since circular sections generally endured a greater number of cycles than the rectangular sections used by Nip *et al.* (2010) and Goggins *et al.* (2005), results are also presented in Table 10 for cycles 11 and 14 in addition to the total accumulated energy. Energy dissipation for each specimen decreased in the cycle prior to failure, which was the case for specimen CF-H-1500 in

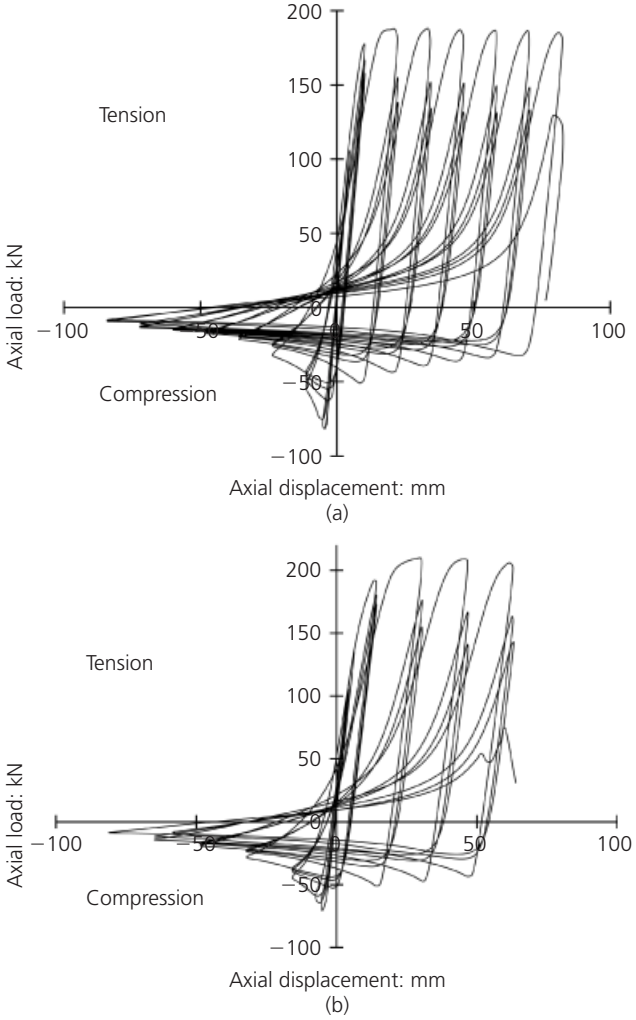

Figure 11. Load–displacement response for 3000 mm hollow specimens: (a) HF-H-3000; (b) CF-H-3000

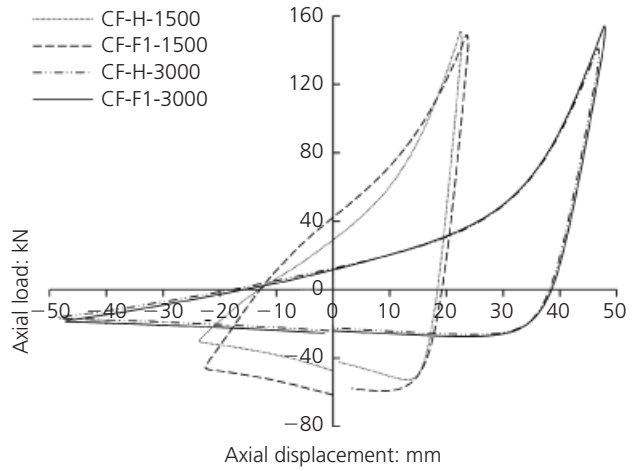

Figure 12. Load–displacement hysteresis for cold-formed members in cycle 13

Specimen ID	Normalised energy dissipation in			Total normalised energy dissipated
	Cycle 8	Cycle 11	Cycle 14	
HF-H-1500	5·3	6·9	8·0	59·1
CF-H-1500	5·0	6·1	2·8	33·1
HF-F1-1500	5·7	7·2	8·4	170·1
HF-F2-1500	4·2	5·8	7·1	84·4
CF-F1-1500	5·2	6·3	7·0	43·1
CF-F2-1500	5·0	6·2	7·0	48·2
HF-H-3000	3·3	3·8	4·3	61·1
CF-H-3000	3·1	3·5	3·8	26·7
HF-F1-3000	3·3	3·9	4·5	68·2
HF-F2-3000	3·3	3·9	4·6	69·9
CF-F1-3000	3·1	3·6	4·0	30·5
CF-F2-3000	3·1	3·7	4·1	32·5

Table 10. Energy dissipated at various stages of testing

cycle 14. The difference in accumulated energy dissipation between hot-finished and cold-formed, filled and hollow specimens, are shown in Figures 13(a) and (b) for the 1500 mm and 3000 mm long braces, respectively. Up to the tenth cycle, little difference is apparent, but the results diverge during later cycles. For both specimen lengths, the hot-finished tubes dissipate a greater amount of energy than the cold-formed. Specimens HF-F1-1500 and CF-F1-1500 show superior energy dissipation to HF-H-1500 and CF-H-1500, respectively, in the later stages of the test, but differences between hollow and filled specimen energy dissipations are almost negligible for 3000 mm specimens, which is reflected in Figure 13(b).

5. Conclusion

Despite the inbuilt efficiency of class 1 circular cross-sections, the results of this research reveal scope for further enhancement of their performance, with concrete infill proving to be an effective possibility. Concrete-filled specimens with a non-dimensional slenderness of less than 1·0 exhibited superior buckling and post-buckling resistances, but the concrete made a lesser contribution to these parameters in specimens with slendernesses close to 2·0. The concrete core increased the maximum tensile resistance for both intermediate and long specimens, however, by between 3·3 and 10%, showing the greatest contribution for intermediate hot-finished tubes. The presence of concrete also increased the number of cycles to failure in all cases, which in turn enhanced the total energy dissipation. For these parameters, the concrete core provides greater enhancement for hot-finished specimens than for cold-formed, despite providing a greater contribution to the cold-formed stub columns than hot-finished.

Distinctions were observed between local deformations of the two specimen lengths, with global buckling behaviour dominating the

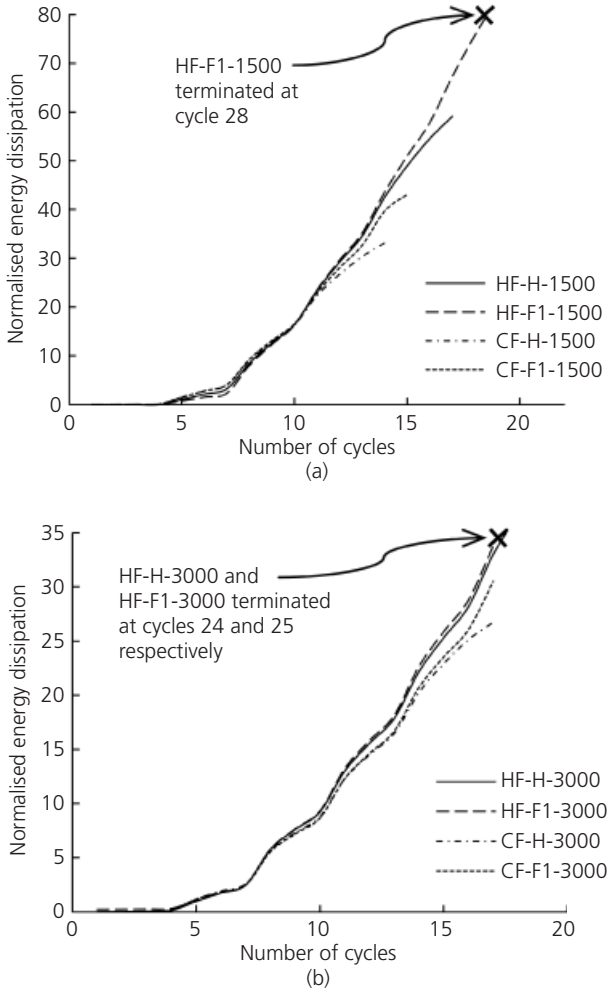

Figure 13. Accumulated energy dissipation: (a) 1500 mm specimens; (b) 3000 mm specimens

3000 mm specimen response and a greater occurrence of local buckling for 1500 mm members. This difference is reflected in the buckling and post-buckling results, but not in the tensile resistances, which are more consistent between intermediate and long braces.

These results provide motivation to conduct further experiments on specimens of intermediary slenderness to establish the deterioration in concrete contribution with increasing slenderness, particularly for values of $\bar{\lambda}$ close to 1·3, the lower limit for cross bracing recommended in BS EN 1998-1 (BSI, 2004b). The cross-sections used for this study had low D/t ratios, which also restricted the potential for concrete contribution to the performance. There is thus an incentive to examine larger D/t ratios of both steel types.

The predicted buckling loads in BS EN 1993-1-1 (BSI, 2005) and EN 1994-1-1 (BSI, 2004a) showed good agreement with the test data for the shorter members, but became more conservative as member length increased. However, for a particular ductility demand under seismic actions, the post-buckling resistance may prove to be the issue of most importance. From the test results, the AISC (2002) guidelines for post-buckling resistance were excessively conservative, while the CSA (1994) allowance over-estimated the capacity. The models proposed by Tremblay (2002) and Nakashima *et al.* (1992) displayed closer agreement with the results, and could potentially improve design efficiency.

Acknowledgements

The authors wish to thank Emeritus Professor Roger Johnson and Professor Toby Mottram from the University of Warwick and Professor Ahmed Elghazouli from Imperial College London for their advice in carrying out this research. The authors are also grateful to Mr Trevor Mustard from Tata Steel for providing sponsorship for this project and for technical assistance received in the University of Warwick laboratories in conducting the experiments. Finally, the first author wishes to acknowledge the recognition received from the Institution of Structural Engineers in awarding first prize to the oral presentation of this research project at the Young Researchers' Conference 2012.

REFERENCES

AISC (American Institute of Steel Construction) (2002) *Seismic Provisions for Structural Steel Buildings*. AISC, Chicago, IL, USA.

Broderick BM, Goggins JM and Elghazouli AY (2005) Cyclic performance of steel and composite bracing members. *Journal of Constructional Steel Research* **61(4)**: 493–514.

BSI (2002) BS EN 12390-3: Testing hardened concrete. Part 3: Compressive strength of test specimens. BSI, Milton Keynes, UK.

BSI (2004a) BS EN 1994-1-1: Design of composite steel and concrete structures. Part 1-1: General rules and rules for buildings. BSI, Milton Keynes, UK.

BSI (2004b) BS EN 1998-1: Design of structures for earthquake resistance. Part 1: General rules, seismic actions and rules for buildings. BSI, Milton Keynes, UK.

BSI (2005) BS EN 1993-1-1: Design of steel structures. Part 1-1: General rules and rules for buildings. BSI, Milton Keynes, UK.

BSI (2009) BS EN ISO 6892-1: Metallic materials – Tensile testing – Method of test at room temperature. BSI, Milton Keynes, UK.

Cai SH (1987) Ultimate strength of concrete-filled tube columns, topics in composite construction in steel and concrete II. *Proceedings of Engineering Foundation Conference*. ASCE, New York, NY, USA, pp. 702–727.

Chan TM and Gardner L (2008) Compressive resistance of hot-rolled elliptical hollow sections. *Engineering Structures* **30(2)**: 522–532.

Chan TM and Gardner L (2009) Flexural buckling of elliptical hollow section columns. *Journal of Structural Engineering* **135(5)**: 546–557.

Chan TM, Gardner L and Law KH (2010) Structural design of

elliptical hollow sections: a review. *Proceedings of the Institution of Civil Engineers – Structures and Buildings* **163(6)**: 391–402.

CSA (Canadian Standard Association) (1994) CAN/CSA-S16 1-94: Limit state design of steel structures. CSA, Rexdale, ON, Canada.

ECCS (European Convention for Constructional Steelwork) (1986) *Recommended Testing Procedure for Assessing the Behaviour of Structural Steel Elements under Cyclic Loads*. ECCS, Brussels, Belgium.

Elchalakani M, Zhao XL and Grzebieta R (2003) Tests of cold-formed circular tubular braces under cyclic axial loading. *Journal of Structural Engineering* **129(4)**: 507–514.

Goggins JM, Broderick BM, Elghazouli AY and Lucas AS (2005) Experimental cyclic response of cold-formed hollow steel bracing members. *Engineering Structures* **27(7)**: 977–989.

Lee C, Grzebieta RH and Zhao XL (2000) The importance of further studies on the capacity evaluation of concrete-filled steel tubes under large deformation cyclic loading. *Structural Failure and Plasticity: Proceedings of the 7th International Symposium on Structural Failure and Plasticity, Melbourne, Australia*, pp. 685–690.

Liu Z and Goel SC (1988) Cyclic load behavior of concrete-filled tubular braces. *Journal of Structural Engineering* **114(7)**: 1488–1506.

Nakashima M, Nishino T, Tsuji B and Iwasa Y (1992) Effect of strain hardening on post-buckling resistance of steel braces. *Proceedings of 3rd Pacific Structural Steel Conference, Tokyo, Japan*, pp. 561–568.

Nip KH, Gardner L and Elghazouli AY (2010) Cyclic testing and numerical modelling of carbon steel and stainless steel tubular bracing members. *Engineering Structures* **32(2)**: 424–441.

Packer JA, Chiew SP, Tremblay R and Martinez-Saucedo G (2010) Effect of material properties on hollow section performance. *Proceedings of the Institution of Civil Engineers – Structures and Buildings* **163(6)**: 375–390.

Tremblay R (2002) Inelastic seismic response of steel bracing members. *Journal of Constructional Steel Research* **58(5/8)**: 665–701.